

Molecular Docking-based Virtual Screening, Molecular Dynamics and Atoms in Molecules (AIM) Studies to Identify Potential Inhibitor against the Extracellular Region of Human Epidermal Receptor 2

H. Moghadam*, B. Ghalami-Choobar* and M. Shafaghat-Lonbar

Department of Chemistry, Faculty of Science, University of Guilan, P. O. Box: 19141, Rasht, Iran

(Received 13 May 2019, Accepted 15 November 2019)

In this study, molecular docking, quantum mechanics and molecular dynamics methods were used to investigate the protein-ligand interactions of the epidermal growth factor receptor 2 (HER2). The virtual screening was performed by docking among 2000 chemicals derived from the ZINC library to find specific inhibitors. Trastuzumab is the active site in the HER2 extracellular domain and the target area. The scoring function was used to calculate the binding affinity of the identified inhibitors to the active site of HER2. Among the inhibitors identified, six ligands were chosen based on their suitable electronic structures and energies. The H-bond interaction energies between six ligands and HER2 were investigated and bond critical points were determined for each bond path between the two corresponding atoms by the quantum theory of atoms in molecules. Root mean square deviation, root mean square fluctuation, the radius of gyration and binding free energy were calculated to evaluate the stability and mobility of the simulated system using molecular dynamics simulation.

Keywords: HER2 drug design, Molecular dynamics, Molecular docking, Quantum theory of atoms in molecules

INTRODUCTION

Breast cancer is one of the major health problems causing a great suffer for humane in almost all countries. It is the most prevalent neoplasia among women and the first cause of death in women in the 40-59 age groups [1]. The epidermal growth factor receptor 2 (HER2) is a member of the EGFR family and its overexpressing occurs from 20% to 25% of invasive breast cancers [2]. Two vitally important kinds of HER2 inhibitors which are currently used in clinical treatment of breast cancer include humanized antibodies directly limiting EGFR/ErbB2 inhibitors and inhibitors of tyrosine kinase (TKIs) competed with ATP in the tyrosine kinase domain of the receptor [3]. In preclinical models, both inhibitors quickly downregulate PI3-AKT,

MAPK, SRC and STAT signaling which subsequently block the growth of tumor cells and human xenografts in nude mice [4]. Trastuzumab is one of the humanized monoclonal antibodies binding to HER2 extracellular domain. A significant number of metastatic breast cancer patients first respond to treatment with trastuzumab; however, within one year of treatment, the resistant to it and the disease will extend. Moreover, the studies performed in recent years have proved the contribution of trastuzumab in one kind of drug-induced cardiac dysfunction [5]. Different molecular mechanisms describing the trastuzumab resistance in breast cancer treatment are as follows: (a) Binding of impaired trastuzumab to HER2 protein: truncated HER2 and epitope masking. (b) Upregulation of HER2 downstream signaling pathways: PTEN loss, increased PI3K/Akt activity, and PDK1 changes. (c) Alternative signaling pathways: increased signaling from HER family and other receptors. (d) Impaired immune-

*Corresponding authors. E-mail: homa.moghadam2013@yahoo.com; b-ghalami@guilan.ac.ir

mediated mechanisms [6]. Immunoprecipitation and Western blot methods have revealed that breast tumor cell lines treated *in vitro* with trastuzumab increase the interaction with CDK2 and levels of p27kip1, leading to a decrease in CDK2 activity [6-7]. HER2-mediated multimerization obstruction causes phosphorylation inhibition, and consequently uncontrolled cell growth and division will be limited. Therefore, a strategic target for breast cancer therapies is the blocking of HER2-mediated signaling [8-11]. The interactions of the protein with different other proteins and protein with different ligands are important for biological functions [12-13]. Prediction of the protein-ligand interaction is used in modern structural-based drug design [12]. The biophysical methods used in protein-ligand and protein-protein interactions study include calorimetric, spectroscopic and structural methods; though, they are expensive techniques [14-16]. Development of computer power and algorithms has made easy the way to study protein-ligand interaction utilizing computational methods. In addition, a computer-aided docking process that identifies the lead compounds by the energy minimizing of intermolecular interactions is a significant approach for structure-based drug designs [17]. A computer method to find a solution to a protein-ligand docking problem comprises two crucial components: a good scoring function and an efficient algorithm for searching conformation and orientation spaces [18-19]. In recent years, Eugene *et al.* have focused on the safety and effectiveness of dual HER2 blockade strategies, such as trastuzumab combined with lapatinib or pertuzumab. For the first time, the term “virtual screening” appeared in a peer-reviewed publication in 1997. Since then the field of virtual screening has become more and more prevalent and has experienced rapid growth in pharmaceutical research. Seetharama *et al.* used an *in silico* screening technique to study the chemical diversity of the compounds designed and exhibited low-energy docked structures for chemical synthesis and biological activity. Shao-Yong Lu *et al.* calculated the electronic interaction energies between several proteins-halogenated complexes using a two-layer quantum mechanics/molecular mechanics (QM/MM) ONIOM method [20]. In 2013, Mirzaie *et al.* combined 3D-QSAR modeling and molecular docking study on multi-acting quinazoline derivatives as HER2 kinase inhibitors [21]. Diana J. Bigler *et al.* calculated the

electronic interaction energies between eight dopaminergic ligands and resveratrol and the SULT1A3 active site using MP2 and M062X with the 6-311+G basis set [22]. Recently, Tripathi *et al.* have used the natural compounds from the ZINC database and performed the computational studies to identify the potential inhibitors of FgTrx1. Based on the binding free energy analyses, they found that compounds with IDs ZINC9312362 and ZINC9312661 could be potential drug candidates to fight against *F. gigantica* parasites [23]. The discovery of innovative leads is a costly and time-consuming procedure. It is estimated that a typical drug discovery cycle, from lead identification through to clinical trials, can take 14 years with a cost of 800 million US dollars [24]. However, expensive and time-consuming process, toxic side effects and the development of drug resistance within a year of treatment, and the appearance of truncated forms of HER2 (p95HER2 and HER2 Δ 16) have shifted the focus of research to targeting the HER2 extracellular region for therapeutics development [25]. Using the computational methods, predicting the interactions of chemical compounds (drugs) with proteins and finding the compounds binding to the target are possible. Then, the binding of these compounds is investigated in the live systems or in the laboratory. In this study, we used virtual screening, molecular docking, quantum mechanics/molecular mechanics (MM/QM) and molecular dynamics (MD) methods to protein-ligand interactions from the different point of views.

METHODS

Materials

Crystal structure of the extracellular region of human HER2 complexed with Herceptin Fab (1N8Z) was retrieved from the Brookhaven protein data bank. All non-polar hydrogen atoms and water molecules were removed, and atom charges were computed using the Gasteiger-Marsili method [26]. Before docking study, the structure was minimized by the steepest descent method implemented in GROMACS 5.0.4 to relax closed contacts [27]. In the present study, to find a special inhibitor for HER2 extracellular region, virtual screening was performed by docking among 2000 molecules from the ZINC database. There are three reasons for using a ZINC database in the

current study; first, the ZINC database represents a much larger database of commercially available compounds for ligand discovery and virtual screening than before. The database is actively maintained and is freely available online (<http://ZINC.docking.org>). Second, ZINC molecules are represented in improved, biologically relevant forms and organized into discovery-relevant subsets such as lead-like and fragment-like. Those are ready for downloading and docking. Third, ZINC can now be used to discover the biological targets for a compound by simple mouse-click, or to find purchasable compounds for a given target, based on literature annotations. We take up each of these results in turn. At over 20 million purchasable molecules, ZINC is the largest database of commercially available compounds for virtual screening. In this study, we used standard ligands file with (B-PO.1.mol2.gz) cod [28].

Molecular Docking

Molecular docking of ZINC library to the active site of HER2 complexed with Herceptin Fab was carried out by Molegro virtual Docker. This software is a virtual screening that works on MolDock scoring function evaluation with a cavity prediction algorithm. Molegro virtual Docker can automatically compute the grid maps [29]. As presented in the introduction, trastuzumab is one of the humanized monoclonal antibodies which binds to HER2 extracellular domain, so we considered a cavity with ($x = 83.00$, $y = 6.00$, $z = -32.44$, $R = 15$) as substrate-binding site [15].

To obtain the validation of docking calculation, Molegro Virtual Docker program used MolDock scoring function evaluation with a cavity prediction algorithm. The MolDock scoring function is based on a piecewise linear potential (plp) and takes into consideration the directionality and charges of hydrogen bonding, defined here as follows:

$$E_{score} = E_{inter} + E_{intra} \quad (1)$$

E_{inter} is protein-ligand interaction energy, defined by the following equation:

$$E_{inter} = \sum_{i \in \text{ligand}} \sum_{j \in \text{protein}} \left[E_{plp(\theta)} + 332.0 \frac{q_i q_j}{4r_{ij}} \right] \quad (2)$$

E_{intra} describes the internal energy of the ligand according to Eq. (3):

$$E_{inter} = \sum_{i \in \text{ligand}} \sum_{j \in \text{protein}} E_{plp(\theta)} + \sum_{\text{flexiblebonds}} A [1 - \cos(m, \theta - \theta_0)] + E_{clash} E_{score} \quad (3)$$

The summation encompasses all heavy atoms in the protein and the ligand as well as any cofactor atoms and water molecule atoms. The second term is torsional energy and is the torsional angle of the bond. E_{clash} term assigns a penalty of 1000 provided that the distance between two heavy atoms is less than 2.0 Å.

Before initiation of docking operation, the molecular structures of the HER2 extracellular domain and ligands, retrieved from the ZINC database, were prepared. The binding site of HER2 was considered as the trastuzumab Restriction (Fig. 1) to this end; charges were calculated by MVD and then appointed to the models. In the initial step of docking operation, the side chain flexibility was set for key residues to predict the binding sites of the HER2 extracellular. MolDock SE was used as a docking algorithm and the energy threshold for pose generation was kept 100.000. Furthermore, similar poses and weak connections were ignored. To this end, the structures of six ligands were evaluated by Molegro virtual Docker with MolDock scoring function; also it was utilized to measure the binding affinity of the identified inhibitor to the active site of the HER2 extracellular domain [30-32]. Then, FAF-Drugs4 program, a free adaptable tool for ADMET (absorption, distribution, metabolism, excretion and toxicity), was used for filtering the electronic compound collections [33].

MD Simulation

All MD simulations were carried out using the GROMACS 5.0.4 package with the AMBER 99SB force field [27]. The partial charges and topology files of inhibitors were produced by ACPYPE which is based on ANTECHAMBER [34]. Each system was hydrated with TIP3P water molecules in a cubic periodic cell [35]. Adequate numbers of chlorine and sodium atoms were added to neutralize the system. Energy minimization was accomplished with the steepest descent integrator and the conjugate gradient algorithm consecutively to achieve a

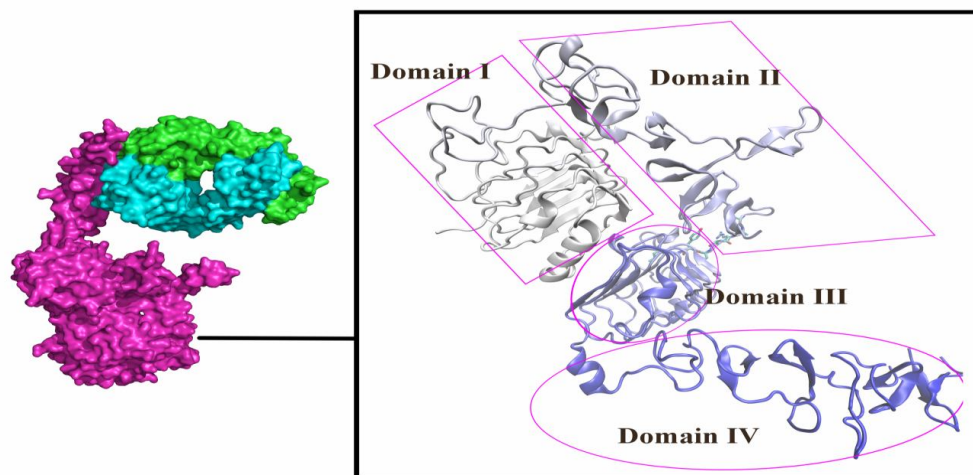


Fig. 1. Surface representation (left side) of extracellular domain of human HER2 (purple) complexed with Herceptin (trastuzumab) Fab (blue and green). Secondary structure presentation of HER2 (right side). Extracellular region of HER2 consists of four distinct domains.

maximum force of less than $1000 \text{ kJ mol}^{-1} \text{ nm}^{-1}$ on any atom. To evaluate short-range, non-bonded interactions, a twin-range cutoff scheme was assigned in which Van der Waals interactions and electrostatic interactions were truncated at 1.4 nm and 0.9 nm, respectively. Particle mesh Ewald (PME) method was utilized to treat the Long-range electrostatic interactions [36,37]. The temperature was fixed at 300 K using velocity rescaling with a stochastic term and coupling time constant of 0.1 ps [38] Parrinello-Rahman barostat with a coupling constant of 2 ps was used to fix pressure at 1.0 atm [39]. All Simulations were conducted with a time step of 2 fs. To constrain all bonds involving hydrogen atoms, a linear constraint solver (LINCS) algorithm was used. Each system was equilibrated under a constant volume (NVT) ensemble (1000 ps) and a constant pressure (NPT) ensemble (1000 ps). All MD simulations were carried out for 30 ns. The trajectories were visualized using VMD software and the standard tools implemented in the GROMACS package [40].

RESULTS AND DISCUSSION

Docking Studies

In the current study, virtual screening was performed by docking among 2000 chemicals derived from ZINC library

to find specific inhibitors against binding site of HER2 extracellular. The scoring function was used to calculate the binding affinity of the identified inhibitors against the binding site of the HER2 extracellular domain; the twenty-three high scores function compounds from virtual screening results obtained are shown in Table 1 [41].

Finally, among the inhibitors found, six ligands having satisfying electronic structure and MolDock energy were chosen. Moreover, it can provide several distribution diagrams of major physicochemical properties of the screened compound libraries. The obtained results for the toxicity of compounds are presented in Table 2. In addition, Table S1 indicates the results for other compounds. In Table S2, details of physico-chemical property filters available in FAF-Drug are listed. Tables S3 and S4 (also Figs. S1 to S4) present oral toxicity prediction, 2D structure, and FAF-Drugs rule for ligand 12, respectively. Also, these values for hits 7, 10, 19, 22 and 23 were reported in supporting information.

Quantum Theory of Atoms in Molecules

Six protein-ligand complexes, cropped within a radius of 15 Å (Molegro virtual Docker), were investigated by using a two-layer quantum mechanics/molecular mechanics (QM/MM) ONIOM method by Gauss View 5.0 software

Table 1. Structures of Potential Inhibitors, their Toxicities and Total Energies

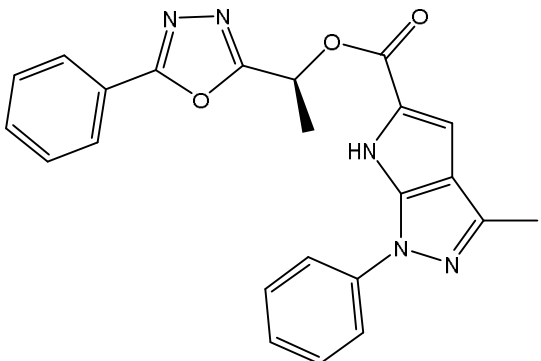
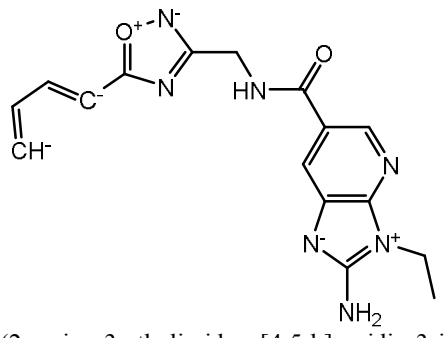
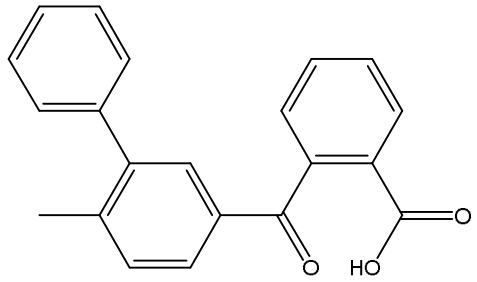
Number	Structure	Tox	E total (Mole dock)
Ligand (1) ID [00]ZINC0852 8998_1	 <p>(S)-1-(5-phenyl-1,3,4-oxadiazol-2-yl)ethyl 3-methyl-1-phenyl-1,6-dihydropyrrolo[2,3-c]pyrazole-5-carboxylate Chemical formula: C₂₃H₁₉N₅O₃</p>	3000 mg kg ⁻¹	-150
Ligand (2) ID Unknown_1_1	 <p>(E)-1-(3-((2-amino-3-ethylimidazo[4,5-b]pyridin-3-ium-1-ide-6-carboxamido)methyl)-1,2,4-oxadiazol-5-yl)buta-1,3-diene-1,4-diide Chemical formula: C₁₆H₁₅N₇O₂₂₋</p>	1190 mg kg ⁻¹	-139
Ligand (3) ID Unknown_1_1	 <p>2-(6-methyl-[1,1'-biphenyl]-3-carbonyl)benzoic acid Chemical formula: C₂₁H₁₆O₃</p>	900 mg kg ⁻¹	-94

Table 1. Continued

Ligand (4) ID Unknown_1_1		1152 mg kg ⁻¹	-183
<p>(S)-N-((R)-1-(5-methyl-4H-1,2,4-triazol-3-yl)ethyl)-2-(o-tolyl)-6,7-dihydro-5H-pyrrolo[1,2-a]imidazole-5-carboxamide Chemical formula: C₁₉H₂₂N₆O</p>			
Ligand (5) ID Unknown_1_1		2112 mg kg ⁻¹	-131
<p>(S)-1-(5-phenyl-1,3,4-oxadiazol-2-yl)ethyl 3-methyl-1-phenyl-4,5-dihydro-1H-pyrazolo[4,3-d]oxazole-5-carboxylate Chemical formula: C₂₂H₁₉N₅O₄</p>			
Ligand (6) ID [00]ZINC1966 4289_1		2082 mg kg ⁻¹	-156
<p>(S)-N-((3-benzyl-1,2,4-oxadiazol-5-yl)methyl)-5-(tert-butyl)-4,5,6,7-tetrahydrobenzo[d]isoxazole-3-carboxamide Chemical formula: C₂₂H₂₆N₄O₃</p>			

Table 1. Continued

Ligand (7) ID [01]ZINC130067 54_1		1400 mg kg ⁻¹	-112
<p>3-(((3S,5S)-3,5-dimethylpiperidin-1-yl)sulfonyl)-N-(5-(p-tolyl)-4H-1,2,4-triazol-3-yl)benzamide Chemical formula: C₂₃H₂₇N₅O₃S</p>			
Ligand (8) ID [00]ZINC085289 98_1		1530 mg kg ⁻¹	-146
<p>A name could not be generated for this structure. Chemical formula: C₂₁H₂₀FN₄O₂</p>			
Ligand (9) ID [00]ZINC Unknown_1_1		1400 mg kg ⁻¹	-186
<p>A name could not be generated for this structure. Chemical formula: C₂₃H₂₄N₅O₃</p>			

Table 1. Continued

Ligand (10) ID [00]ZINC0852 8998_1		2580 mg kg ⁻¹	-131
Ligand (11) ID [00]ZINC Unknown_1_1		1000 mg kg ⁻¹	-161
Ligand (12) ID [00]ZINC Unknown_1_1		1000 mg kg ⁻¹	-141
Ligand (13) ID Unknown_1_1		2000 mg kg ⁻¹	-122

Table 1. Continued

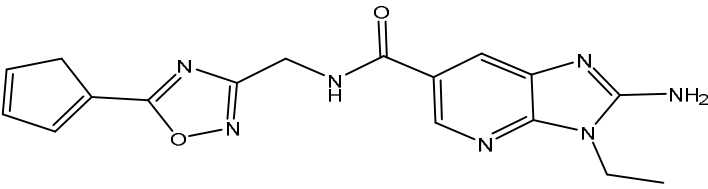
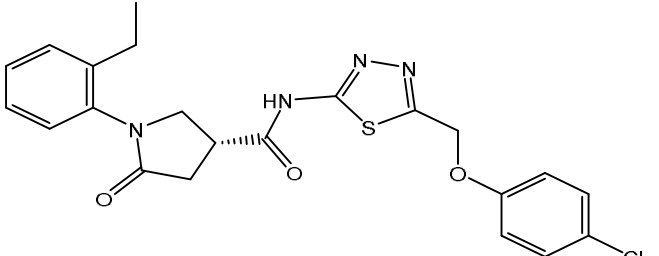
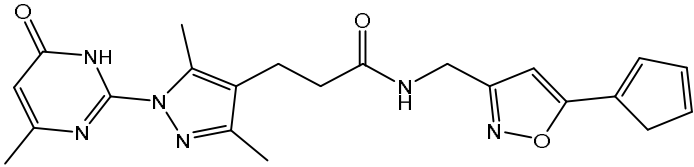
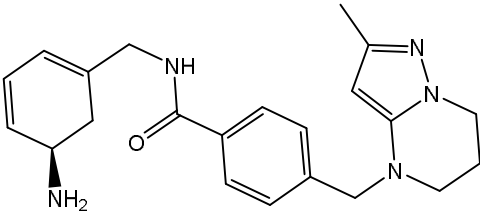
Ligand (14) ID Unknown_1_1	 <p data-bbox="421 680 1072 768">2-amino-N-((5-(cyclopenta-1,3-dien-1-yl)-1,2,4-oxadiazol-3-yl)methyl)-3-ethyl-3H-imidazo[4,5-b]pyridine-6-carboxamide Chemical formula: C₁₇H₁₇N₇O₂</p>	1400 mg kg ⁻¹	-120
Ligand (15) ID [00]ZINC2037 2088_1	 <p data-bbox="408 1095 1086 1189">(S)-N-(5-((4-chlorophenoxy)methyl)-1,3,4-thiadiazol-2-yl)-1-(2-ethylphenyl)-5-oxopyrrolidine-3-carboxamide Chemical formula: C₂₂H₂₁ClN₄O₃S</p>	2580 mg kg ⁻¹	-125
Ligand (16) ID Unknown_1_1	 <p data-bbox="384 1447 1107 1563">N-((5-(cyclopenta-1,3-dien-1-yl)isoxazol-3-yl)methyl)-3-(3,5-dimethyl-1-(4-methyl-6-oxo-1,6-dihydropyrimidin-2-yl)-1H-pyrazol-4-yl)propanamide Chemical formula: C₂₂H₂₄N₆O₃</p>	1300 mg kg ⁻¹	-146
Ligand (17) ID Unknown_1_1	 <p data-bbox="392 1868 1101 1953">(R)-N-((5-aminocyclohexa-1,3-dien-1-yl)methyl)-4-((2-methyl-6,7-dihydropyrazolo[1,5-a]pyrimidin-4(5H)-yl)methyl)benzamide Chemical formula: C₂₂H₂₇N₅O</p>	1000 mg kg ⁻¹	-123

Table 1. Continued

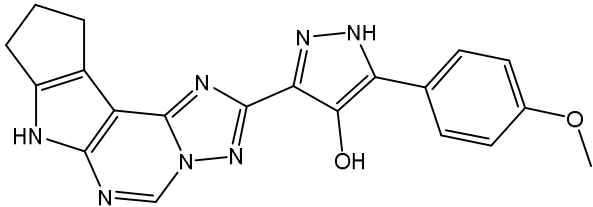
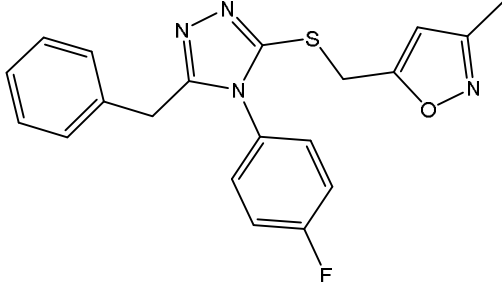
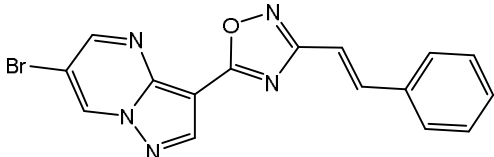
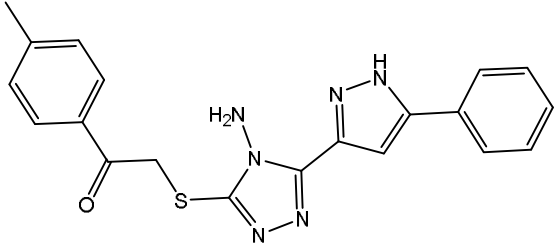
Ligand (18) ID Unknown_1_1	 <p data-bbox="432 696 1043 813">3-(4-methoxyphenyl)-5-(7,8,9,10-tetrahydrocyclopenta[4,5]pyrrolo[3,2-e][1,2,4]triazolo[1,5-c]pyrimidin-2-yl)-1H-pyrazol-4-ol Chemical formula: C₂₀H₁₇N₇O₂</p>	3200 mg kg ⁻¹	-170
Ligand (19) ID [00]ZINC0852 8998_1	 <p data-bbox="467 1167 1019 1254">5-(((5-benzyl-4-(4-fluorophenyl)-4H-1,2,4-triazol-3-yl)thio)methyl)-3-methylisoxazole Chemical formula: C₂₀H₁₇FN₄OS</p>	1000 mg kg ⁻¹	-151
Ligand (20) ID Unknown_1_1	 <p data-bbox="421 1480 1067 1570">(Z)-5-(6-bromopyrazolo[1,5-a]pyrimidin-3-yl)-3-styryl-1,2,4-oxadiazole Chemical formula: C₁₆H₁₀BrN₅O</p>	800 mg kg ⁻¹	-146
Ligand (21) ID [00]ZINC0910 8756_1	 <p data-bbox="416 1883 1074 1960">2-((4-amino-5-(5-phenyl-1H-pyrazol-3-yl)-4H-1,2,4-triazol-3-yl)thio)-1-(p-tolyl)ethanone Chemical formula: C₂₀H₁₈N₆OS</p>	1500 mg kg ⁻¹	-160

Table 1. Continued

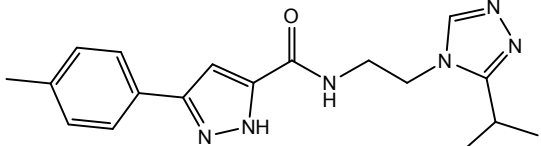
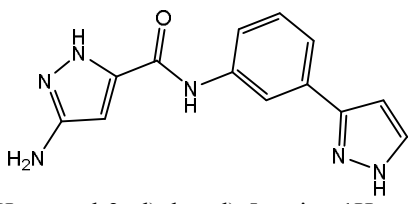
Ligand (22) ID [00]ZINC8142 1556_1		1000 mg kg ⁻¹	-34.2485
N-(2-(3-isopropyl-4H-1,2,4-triazol-4-yl)ethyl)-3-(p-tolyl)-1H-pyrazole-5-carboxamide Chemical formula: C ₁₈ H ₂₂ N ₆ O			
Ligand (23) ID [00]ZINC3849 0087_1		2000 mg kg ⁻¹	-141
N-(3-(1H-pyrazol-3-yl)phenyl)-5-amino-1H-pyrazole-3-carboxamide Chemical formula: C ₁₃ H ₁₂ N ₆ O			

Table 2. The 2D Structures, Toxicities and Docking Energies of Six Hits

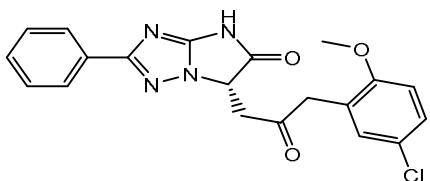
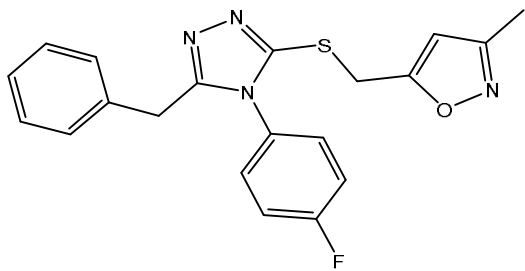
Compound	Abbreviation	Structure	Tox	E (kJ mol ⁻¹)
Ligand (12) ID [00]ZINC Unknown_1_1	A		1000 mg kg ⁻¹	-435.8315
(S)-6-(3-(5-chloro-2-methoxyphenyl)-2-oxopropyl)-2-phenyl-4H-imidazo[1,2-b][1,2,4]triazol-5(6H)-one Chemical formula: C ₂₀ H ₁₇ ClN ₄ O ₃				
Ligand (19) ID [00]ZINC08528 998-1	B		1000 mg kg ⁻¹	-174.3339
5-(((5-benzyl-4-(4-fluorophenyl)-4H-1,2,4-triazol-3-yl)thio)methyl)-3-methylisoxazole Chemical formula: C ₂₀ H ₁₇ FN ₄ OS				

Table 2. Continued

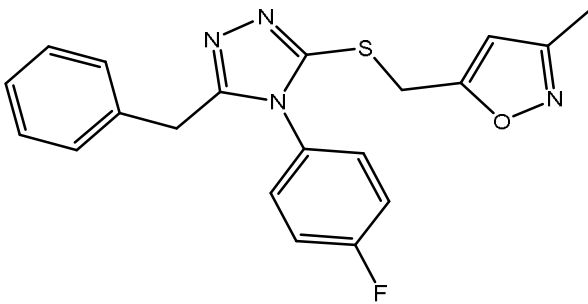
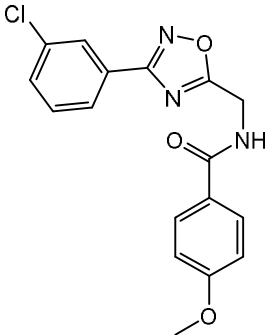
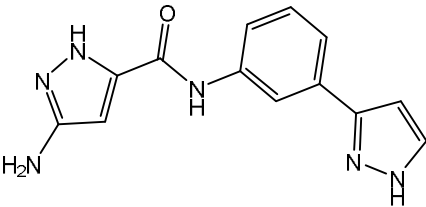
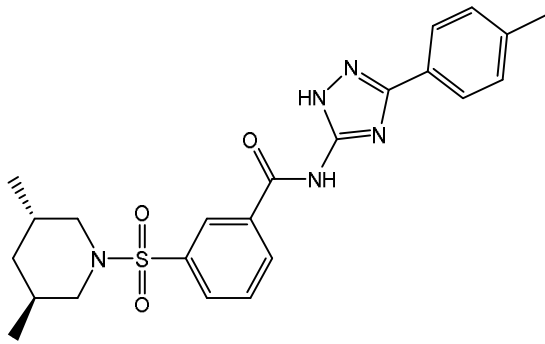
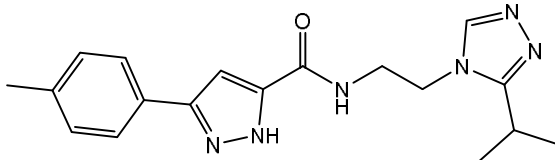
Ligand (19) ID [00]ZINC08528998-1	B	 <p>5-(((5-benzyl-4-(4-fluorophenyl)-4H-1,2,4-triazol-3-yl)thio)methyl)-3-methylisoxazole Chemical formula: C₂₀H₁₇FN₄OS</p>	1000 mg kg ⁻¹	-174.3339
Ligand (10) ID [00]ZINC08528998_1	\ C	 <p>N-((3-(3-chlorophenyl)-1,2,4-oxadiazol-5-yl)methyl)-4-methoxybenzamide Chemical formula: C₁₇H₁₄ClN₃O₃</p>	2580 mg kg ⁻¹	-153.7077
Ligand (23) ID [00]ZINC38490087_1	D	 <p>N-(3-(1H-pyrazol-3-yl)phenyl)-5-amino-1H-pyrazole-3-carboxamide Chemical formula: C₁₃H₁₂N₆O</p>	2000 mg kg ⁻¹	-133.9403

Table 2. Continued

Ligand (7) ID [01]ZINC13006754_1	E		1400 mg kg ⁻¹	-98.1656
<p>3-(((3S,5S)-3,5-dimethylpiperidin-1-yl)sulfonyl)-N-(5-(p-tolyl)-4H-1,2,4-triazol-3-yl)benzamide Chemical formula: C₂₃H₂₇N₅O₃S</p>				
Ligand (22) ID [00]ZINC81421556_1	F		1000 mg kg ⁻¹	-34.2485
<p>N-(2-(3-isopropyl-4H-1,2,4-triazol-4-yl)ethyl)-3-(p-tolyl)-1H-pyrazole-5-carboxamide Chemical formula: C₁₈H₂₂N₆O</p>				

[42]. Then, the structures of the six ligands bound in the active site were optimized with Gaussian 0.3 software [43]. The hydrogen binding between ligands and protein, cropped within a radius of 3 Å, are shown in Fig. 2 [20].

AIM Analysis on the Bond Critical Points

Quantum-mechanical calculations were carried out to optimize all geometries by the Gaussian03 program [44] using the Becke3-Lee-Yang-Parr (B3LYP) functional [45,46] supplemented with the standard 6-311++G(d,p) basis set [47]. To evaluate the intramolecular interaction energy, the following equation, given by Espinosa *et al.* [48], has been used. According to the properties of electron density distribution in the bond critical points (BCPs), we have $E = 0.5 V$ [49]; where V is the value of the local potential energy at the BCP for interaction. The theoretical calculations of delocalization index between H, N and H,

O and transition state as well as topological analyses of electron density were performed using the AIM theory implemented in the AIM All program [50]. The Bader theory is a useful tool to analyze hydrogen bonds. The analysis of the BCPs' (Bond critical points) properties has generally been conducted to estimate the nature of the hydrogen bonds [49,51-55].

In this study, the H-bond interaction energies between six ligands and HER2 extracellular domain IV were investigated. BCPs were identified in the QM layer for each bond path between the two corresponding atoms. This result indicates that the ligand can form multifaceted hydrogen-bonding interactions with the residues. The properties at the BCPs were analyzed in terms of some parameters such as the electron density (ρ_b) and its Laplacian ($\nabla^2\rho_b$), and the electron energy density (H_b). The following components of H_b have been also included: the kinetic electron energy

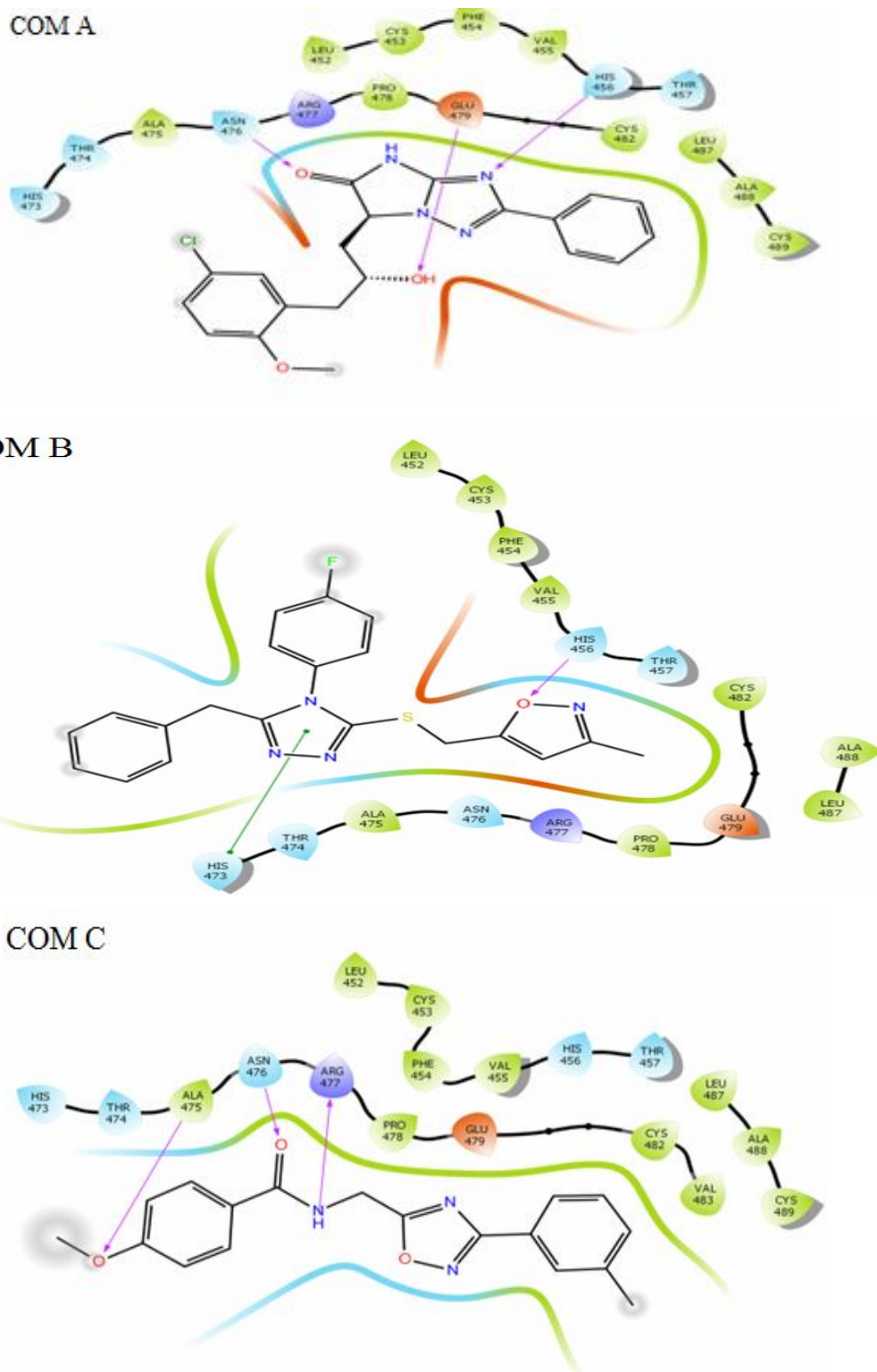


Fig. 2. Molecular docking interactions for protein with six ligands which having higher energy in both docking score and binding energy calculations.

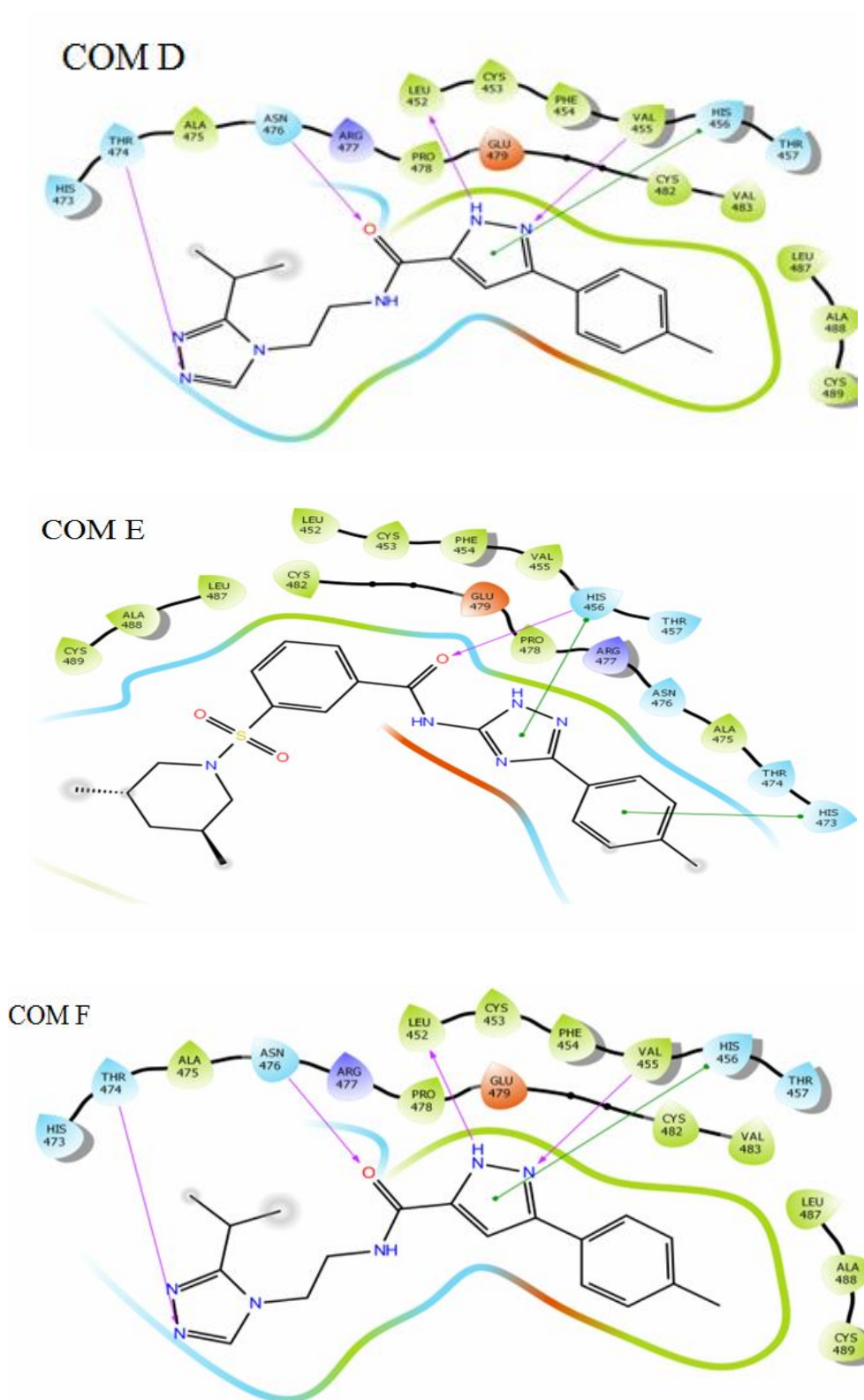


Fig. 2. Continued.

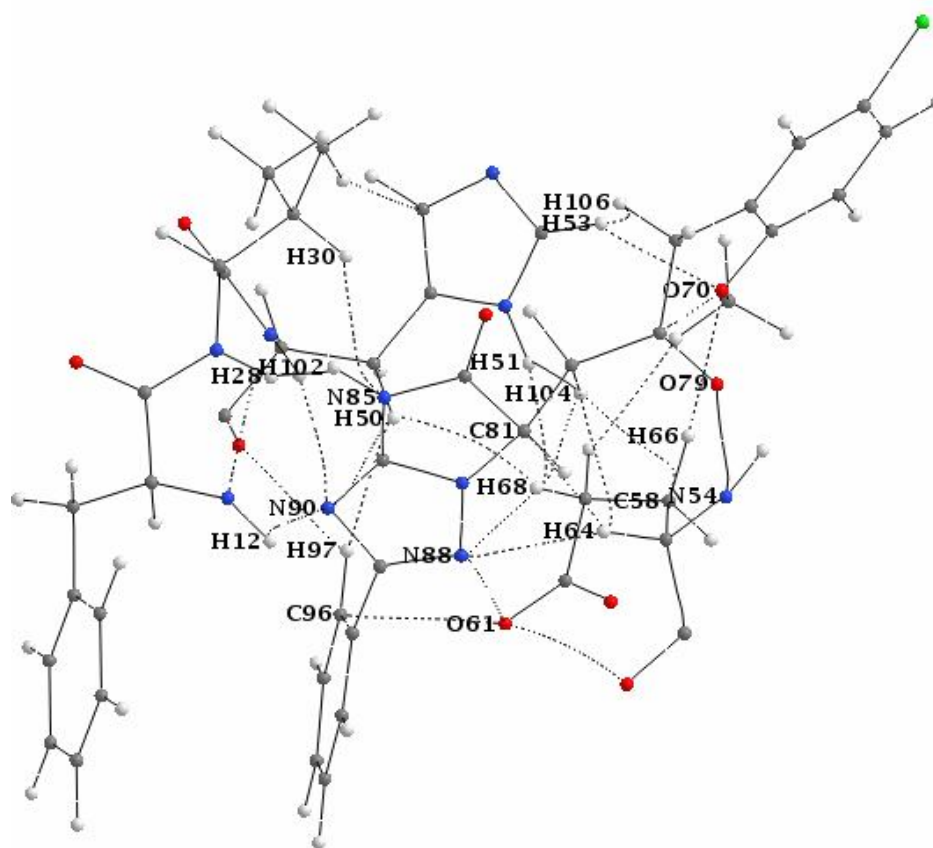


Fig. 3. Amino acid residues which form the active site of the HER2/ligand 12(A) at 15 Å distance away from A.

density (G_b) and the potential electron energy density (V_b). The AIM results were examined for the ligand-protein bond in the QM layers after ONIOM calculations for all the complexes. In the X-bonding parts, as shown in Tables 3-9, it can be seen that the values of ρ_b and $\nabla^2\rho_b$ were calculated to be in the range of 0.0018-0.0924 au and 0.0060-0.1371 au, respectively. These values at BCPs are within the accepted ranges for H-bonding interactions, suggesting that H-bonding interactions occur in these systems. The electron energy density, H_b , was considered as an index to gain a better understanding of non-covalent interactions. The signs of the H_b values at the BCPs determine whether the dominant interaction is electrostatic ($H_b > 0$) or covalent ($H_b < 0$) [56]. The parameters such as the Laplacian of the electron density, $\nabla^2\rho$, the electron energy density, H_C , the sum of the kinetics electron energy density, G_C , and the potential electron energy density, V_C , as well as $-G_C/V_C$, are driven from the Bader theory, implying the interaction type

and changing stability of the bonds after molecular rotation, intermolecular or intra-molecular interactions. For a negative value of Laplacian, $\nabla^2\rho < 0$, the interaction is completely covalent. If both $\nabla^2\rho$ and H_C are simultaneously positive ($\nabla^2\rho > 0$, $H_C > 0$), the interaction is categorized among the closed shell interactions; most hydrogen bonds and Van der Waals interactions belong to this category. If $\nabla^2\rho$ is positive while H_C is negative, and the $-G_C/V_C$ is smaller than 1, the nature of the interaction is considered as partly covalent [57].

AIM analysis on the BCP for Protein-Ligand12 (COM A). The strong interactions between Glu479 and ligand indicate the fundamental role of this residue in interaction with ligand. The interaction of N54 from amino acid with O79 of ligand having a significant amount of energy is a quasi-covalent interaction. The two interactions of O61 with C96 and N88 and also interactions of C58-H104 and H64-C81 have a Van der Waals nature. The other

interactions of this residue with ligands are H-bond type. Considering Val455 residue, H28 from amino acid has an interaction with H102 of imidazole ring. Moreover, there is an interaction between the residue's H30 with N85 of imidazole group. Imidazole ring causes the stability of these interactions. From the obtained topological values, they can be considered as quasi-covalent interactions. His456 residue has seven interactions with ligand 12 including H50-H97, H50-H68, H51-H68, H53-O70, H50-N90, H51-H104 and H53-H104 (Fig. 3). Among them, the H51-H104 interaction is a strong dihydrogen interaction. In another residue, Phe454, the only interaction is the interaction of H12 with N90 of ligand. The value of interaction energy and length is $-13.517 \text{ kJ mol}^{-1}$ and 4.532 \AA , respectively. The obtained topological values show that this is a H-bond type interaction; this information is depicted in Table 3.

Also, Figs. 25 to 28 depict the residues located at the active site near the COM B, COM C, COM D, COM E, and COM F at 15 \AA , respectively. Moreover, atom energies obtained through Molegro virtual docker, docking results and energy overview are listed in Tables S15, S16 and S17 for COM B. The similar results were reported for the COM B, COM C, COM D, COM E, and COM F in supporting information.

Considering the energy values obtained, the orders of interactions based on stability are as follows:

E: Glu479 (N54-O79) > val455 (H28-H102) > His456 (H51-H104) > His456 (H53-O70) > Glu479 (O61-C96) > Phe454 (H30-N85) > Phe454 (H12-N90) > Phe454 (H64-N88) > Glu479 (H68-N88) > Glu479 (H66-O70) > His456 (H51-H68) > Glu479 (H64-C81) > His456 (H53-H106) > Glu479 (C58-H104) > Glu479 (O61-N88) > His456 (H50-H97) > His456 (H50-H68) > His456 (H50-N90)

AIM analysis on the BCP for Protein-Ligand19 (COM B). There are two interactions between val455 and ligand 19. The first one is the interaction of H8 from amine group with N53 from imidazole ring and the second is the interaction between H10 of amino acid and O52 of oxadiazole ring. Here, the interaction energies and lengths are -21.216 and $-37.324 \text{ kJ mol}^{-1}$ and 4.122 \AA , 3.622 \AA , respectively. One of the interactions of His456 residue with the ligand is H33-S55 interaction, with the interaction energy $-17.848 \text{ kJ mol}^{-1}$, indicating that this residue has stronger interaction than Asn 476 and val455. The

interaction of H33 and H27 from imidazole ring with N53 from oxadiazole ring and S55 respectively leads to further stability of His 456 residue, as depicted in Table 4. Based on the energy values obtained, the order of interactions based on stability is as follows:

His456 (H27-N53) > val455 (H10-O52) > val455 (H8-N53) > His456 (H33-S55) > Asn476 (H45-H87) > Asn476 (H42-N58) > Asn476 (H45-N57) > His456 (H12-C24) > His456 (N23-O52) > Asn476 (O37-H79) > His456 (H30-N53) > Asn476 (O37-H80) > Asn476 (N34-H79) > Asn476 (H47-H86)

AIM analysis on the BCP for Protein-Ligand10 (COM C).

There are three strong interactions between His456 and imidazole ring of the ligand. In two interactions, H31 and H34 from residue react with N64 of imidazole ring with interaction energies $-8.394 \text{ kJ mol}^{-1}$ and $-16.918 \text{ kJ mol}^{-1}$, and distances 4.8595 \AA , 4.228 \AA , respectively. The calculated values of ρ , $\nabla^2\rho$ and H imply to hydrogen bonding type of these interactions. The third interaction is the interaction of N27 of methyl group with O63 of ligand having energy and distance of, respectively, $-15.092 \text{ kJ mol}^{-1}$ and 5.487 \AA . Considering the BCP values, it can be realized that this is a Van der Waals interaction. In another residue, Asn476, H49 and H51 simultaneously interact with O68 of carbonyl group which possess energies $-8.234 \text{ kJ mol}^{-1}$ and $-43.729 \text{ kJ mol}^{-1}$ and distance 5.445 \AA , 3.411 \AA , respectively. Based on the topological values, these interactions can be regarded as hydrogen bonding. The third interaction of Asn476 belongs to C70-H46 which is a weak Van der Waals interaction. In the case of Phe454 residue, the interaction of H12 and H87 is associated with the energy value $-40.842 \text{ kJ mol}^{-1}$ and distance 2.847 \AA . Herein, $\nabla^2\rho < 0$ and $-G/V$ is smaller than unity representing that although this interaction is dihydrogen, it is partially covalent in nature. Also, the interaction occurring between H12 with N61 of oxadiazole ring has energy and distance of, $-16.294 \text{ kJ mol}^{-1}$ and 4.379 \AA , respectively, and is a hydrogen bonding interaction. Finally, the interaction of C8 with H88 of ligand has energy and distance of $-3.190 \text{ kJ mol}^{-1}$ and 5.741 \AA , respectively. According to the BCP values, it can be considered as a Van der Waals interaction. This information is depicted in Table 5. From the energy values obtained, the order of interactions based on stability is as follows:

Table 3. Topological Properties of the Ligand 12-HER2(COM A) Bond Critical Points (XBCPs) for all the Systems Considered

COM A	Atoms	BPL	ρ	$\nabla^2\rho$	G	V	H	-G (V)	E (kJ mol ⁻¹)
Phe454	H12-N90	4.5322	0.0153	0.0529	0.0118	-0.0104	0.0014	1.1356	-13.5174
val455	H28-H102	2.2556	0.0621	0.1742	0.0537	-0.0639	-0.0102	0.8408	-83.0531
	H30-N85	4.7110	0.0154	0.0604	0.0130	-0.0110	0.0021	1.1869	-14.2766
His456	H50-H97	4.4320	0.0057	0.0213	0.0040	-0.0026	0.0013	1.5045	-1.9357
	H50-N90	6.1724	0.0030	0.0102	0.0020	-0.0015	0.0005	1.3714	-3.4398
	H51-H104	3.0103	0.0286	0.0937	0.0247	-0.0260	-0.0013	0.9502	-1.9006
	H53-O70	4.3041	0.0167	0.0567	0.0136	-0.0131	0.0006	1.0430	-33.8026
	H51-H68	4.0680	0.0123	0.0456	0.0096	-0.0078	0.0017	1.2263	-10.2219
	H53-H106	4.16331	0.01156	0.0463	0.0093	-0.0070	0.0022	1.3236	-9.1377
Glu479	H50-H68	5.1381	0.0035	0.0117	0.00221	-0.0014	0.0007	1.4869	-1.9357
	C58-H104	5.3135	0.0095	0.0394	0.0079	-0.0060	0.0019	1.3182	-7.8429
	H64-C81	4.7291	0.0113	0.0465	0.0096	-0.0076	0.0020	1.2618	-9.1377
	H64-N88	4.4067	0.0148	0.0505	0.0113	-0.0100	0.0013	1.1278	-16.9754
	H66-O70	4.5524	0.0113	0.0391	0.0091	-0.0085	0.0006	1.0756	-7.8429
	H68-N88	4.4475	0.0147	0.0487	0.0111	-0.0100	0.0011	1.1095	-9.9203
	N54-O79	3.5529	0.0924	0.4686	0.1238	-0.1305	-0.0067	0.9489	-13.0598
	O61-C96	5.0036	0.0170	0.0612	0.0136	-0.0118	0.0017	1.1478	-11.0396
	O61-N88	5.7166	0.0087	0.0275	0.0064	-0.0059	0.0005	1.0805	-12.9935
	N54-O79	3.5528	0.0924	0.46860	0.1238	-0.1304	-0.0066	0.9488	-169.6461
O61-C96	5.00356	0.01695	0.06124	0.01356	-0.01181	0.00174	1.147837	-15.3621	
O61-N88	5.7165	0.00873	0.0275	0.00640	-0.0059	0.00047	1.080465	-7.7064	

E: Asn476 (H51-O68) > Phe454 (H12-H87) > His456 (H34-N64) > Phe454 (H12-N61) > His456 (N27-O63) > His456 (H31-N64) > Asn476 (H49-O68) > Phe454 (C8-H88) > Asn476 (H46-C70)

AIM analysis on the BCP for Protein-Ligand23 (COM D). The single interaction of Leu452 with ligand23

is a hydrogen bond occurring between O4 and H65 of imidazole group. In Val455, there is an interaction between H27 and N63 with energy and distance of -37.961 kJ mol⁻¹ and 3.603 Å, respectively. This interaction is dihydrogen and partial covalent in nature. Besides, H29 interacts with N64 and O59 of carbonyl group. The values

Table 4. Topological Properties of the Ligand 19-HER2(COM B) Bond Critical Points (XBCPs) for all the Systems Considered

COM B	Atoms	BPL	ρ	$\nabla^2\rho$	G	V	H	-G (V)	E (kJ mol ⁻¹)
His456	H12-C24	4.879014	0.009381	0.031392	0.006455	-0.005061	0.001394	1.2754396	-6.5793
	H27-N53	3.412361	0.040979	0.137123	0.035576	-0.036872	-0.001296	0.9648514	-47.9336
	H30-N53	5.674445	0.005251	0.017176	0.003605	-0.002917	0.000688	1.2358588	-3.7921
	H33-S55	4.736301	0.019138	0.065058	0.014997	-0.013729	0.001268	1.0923592	-17.8477
	N23-O52	6.215581	0.006227	0.019575	0.004627	-0.00436	0.000267	1.0612385	-5.668
val455	H10-O52	3.621783	0.031246	0.120549	0.029424	-0.028711	0.000713	1.0248337	-37.3243
	H8-N53	4.122437	0.020196	0.07544	0.01759	-0.01632	0.00127	1.0778186	-21.216
Asn476	H42-N58	4.741752	0.009238	0.032851	0.007186	-0.006159	0.001027	1.1667478	-8.0067
	H45-H87	3.757136	0.011449	0.042271	0.008977	-0.007387	0.00159	1.215243	-9.6031
	H45-N57	4.942029	0.009546	0.029255	0.006487	-0.005661	0.000826	1.1459106	-7.3593
	H47-H86	5.25197	0.002375	0.009721	0.001706	-0.000983	0.000723	1.7355036	-1.2779
	N34-H79	5.959262	0.002667	0.009633	0.001855	-0.001302	0.000553	1.4247312	-1.6926
	O37-H79	5.246521	0.004636	0.019439	0.003909	-0.002958	0.000951	1.321501	-3.8454
	O37-H80	5.799893	0.00279	0.012565	0.002412	-0.001683	0.000729	1.4331551	-2.1879

Table 5. Topological Properties of the Ligand 10-HER2(COM C) Bond Critical Points (XBCPs) for all the Systems Considered

COM C	Atoms	BPL	ρ	$\nabla^2\rho$	G	V	H	-G (V)	E (kJ mol ⁻¹)
Phe454	C8-H88	5.7408	0.0055	0.0171	0.0034	-0.0025	0.0009	1.3696	-3.1902
	H12-H87	2.8468	0.0332	0.0990	0.0281	-0.0314	-0.0033	0.8941	-40.8421
	H12-N61	4.3795	0.0168	0.0650	0.0144	-0.0125	0.0019	1.1484	-16.2942
His456	H31-N64	4.8595	0.0099	0.0335	0.0074	-0.0065	0.0010	1.1491	-8.3941
	H34-N64	4.2282	0.0178	0.0600	0.0140	-0.0130	0.0010	1.0761	-16.9182
	N27-O63	5.4873	0.0148	0.0616	0.0135	-0.0116	0.0019	1.1636	-15.0917
Asn476	H46-C70	6.5278	0.0022	0.0060	0.0011	-0.0008	0.0004	1.4679	-1.014
	H49-O68	5.4452	0.0101	0.0383	0.0079	-0.0063	0.0016	1.2550	-8.2342
	H51-O68	3.4108	0.0355	0.1335	0.0331	-0.0329	0.0002	1.0076	-43.729

of energy and distance for these two interactions are, respectively, -21.056, -5.890 kJ mol⁻¹ and 4.084 Å and 5.232 Å. From the data in Table 6, these interactions can classify as Van der Waals. The other interaction belongs to a hydrogen bond between H30 of methyl group H30 and O59 having energy and distance of -5.147 kJ mol⁻¹ and 5.283 Å, respectively. Considering Asn476, the O39 of residue has interaction with phenol and imidazole ring. These interactions belong to O39-C53 and O39-N82, respectively. Both of these interactions have Van der Waals nature. Moreover, H49 from amid group and H47 interact with O59 of carbonyl group. The values of interaction energy and distance are -28.1346, -13.253 kJ mol⁻¹ and 3.690 Å, 4.462 Å, respectively. The achieved topological parameters infer that the hydrogen bond occurring between H49 and O59 is stronger than H47-O59 one. Finally, the interaction of H44 with C51 is weak Van der Waals interaction with energy and length -3.427 kJ mol⁻¹ and 5.507 Å, respectively. According to the obtained values of energy, the order of interactions based on stability is as follows:

E val455 (H27-N63) > E Asn476 (H49-O59) > E val455 (H29-N64) > E Asn476 (H47-O59) > E Leu452 (O4-H65) > E val455 (H29-O59) > E Asn476 (O39-N82) > Asn476 (H44-C51) > Asn476 (O39-C53)

AIM analysis on the BCP for Protein-Ligand 7(COM E). In COM E, three residues interact with ligand. His 456 has three interactions with ligand as H47-O71, H53-C58 and H51-N64 having interaction energies and -23.356, -12.152, -16.441 kJ mol⁻¹ and distances 3.897 Å, 5.228 Å, and 4.336 Å, respectively. From the BCP parameters presented in Table 7, the first interaction between H47 of amid group and O71 of carbonyl group is a hydrogen bond interaction. Similarly, the other interaction which is between H51 and N64 of imidazole ring is also hydrogen bonding in type. However, the interaction of H53 with C58 is Van der Waals in nature. In another residue, Phe454, the only interaction is N1 with O71 having the energy of -13.684 kJ mol⁻¹ and distance of 5.516 Å. Here, the BCP parameters show that the nature of this interaction is Van der Waals. Two interactions of val455 residue include H30-N68 with the energy of -12.549 kJ mol⁻¹ and distance of 4.464 Å and interaction of N21-O71 with energy and distance of -11.440 kJ mol⁻¹ and 5.516 Å, respectively.

From the information of BCP parameters, it can be deduced that the first is a hydrogen bonding interaction but the latter is a weak Van der Waals. This interaction is a hydrogen bonding interaction. Regarding the energy values obtained, the order of interactions based on stability is as follows:

E: His456 (H47-O71) > His456 (H51-N64) > Phe454 (N1-O71) > val455 (H30-N68) > His456 (H53-C58) > val455 (N21-O71)

AIM analysis on the BCP for Protein-Ligand 22(COM F). There are four interactions in Asn476 residue with ligand including O23-H65, O23-H68, H31-O50 and H33-O50, the energies of interactions are: -1.266, -1.195, -11.657 and -9.396 kJ mol⁻¹, respectively. The BCP values for these interactions imply to their hydrogen bond nature. The only interaction of Leu452 with the ligand is O4-H47 having energy and distance -9.841 kJ mol⁻¹ and 4.489 Å, respectively. From the BCP parameters given in Table 8, it can be concluded that this is a hydrogen bond interaction. From the energy data obtained, the order of interactions based on stability is as follows:

E: val455 (H27-N63) > Asn476 (H49-O59) > val455 (H29-N64) > Asn476 (H47-O59) > Leu452 (O4-H65) > val455 (H29-O59) > Leu452 (O39-N82) > val455 (H44-C51) > Asn476 (O39-C53)

The AIM results indicated that the best pose of ligand 12 in the binding site of HER2 extracellular has a binding affinity of -435.831 kJ mol⁻¹ and also the weakest pose is related to ligand 22 that has a binding affinity of -34.248 kJ mol⁻¹, the results are shown in Table 9. From the obtained quantum computational results point of view, the complex of COM A has stronger interactions than others and the weaker interactions belong to COM F.

Flexibility and Mobility Study

Analyzing the MD simulation trajectories provides a better picture of the overall stability and behavior of the protein. Root mean square deviation (RMSD), root mean square fluctuation (RMSF) and radius of gyration (Rg) are useful parameters to evaluate the stability and mobility of the simulated system.

Root mean square deviation (RMSD). After docking studies, COM A, COM B, COM C (with -435.831, -174.334 and -153.708 kJ mol⁻¹ docking energies, respectively) were

Table 6. Topological Properties of the Ligand 23-HER2(COM D) Bond Critical Points (XBCPs) for all the Systems Considered

COM D	Atoms	BPL	ρ	$\nabla^2\rho$	G	V	H	-G (V)	E (kJ mol ⁻¹)
Leu452	O4-H65	4.5022	0.0117	0.0482	0.0107	-0.0093	0.0013	1.1440	-12.1524
val455	H27-N63	3.6030	0.0335	0.1082	0.0281	-0.0292	-0.0011	0.9631	-37.9613
	H29-N64	4.0844	0.0211	0.0720	0.0171	-0.0162	0.0009	1.0559	-21.0561
	H29-O59	5.2324	0.0068	0.0246	0.0053	-0.0045	0.0008	1.1788	-5.8903
	H30-O59	5.2828	0.0063	0.0240	0.0050	-0.0040	0.0010	1.2579	-5.1467
Asn476	H44-C51	5.5073	0.0055	0.0180	0.0036	-0.0026	0.0009	1.3536	-3.4268
	H47-O59	4.4619	0.0134	0.0456	0.0108	-0.0102	0.0006	1.0596	-13.2535
	H49-O59	3.6896	0.0238	0.0950	0.0227	-0.0216	0.0011	1.0487	-28.1346
	O39-C53	6.3858	0.0047	0.0154	0.0032	-0.0026	0.0006	1.2302	-3.4216
	O39-N82	6.3662	0.0040	0.0147	0.0032	-0.0027	0.0005	1.1840	-3.497

Table 7. Topological Properties of the Ligand 7-HER2 (COM E) Bond Critical Points (XBCPs) for all the Systems Considered

COM E	Atoms	BPL	ρ	$\nabla^2\rho$	G	V	H	-G (V)	E (kJ mol ⁻¹)
His456	H30-N68	4.463998	0.014006	0.047613	0.010778	-0.009653	0.001125	1.11654408	-12.5489
	H31-H108	4.770611	0.003649	0.013368	0.002401	-0.001461	0.00094	1.643394935	-1.8993
	H32-C44	4.877241	0.009576	0.031681	0.006553	-0.005186	0.001367	1.263594292	-6.7418
	H47-O71	3.896752	0.020534	0.074138	0.01825	-0.017966	0.000284	1.015807637	-23.3558
	H51-N64	4.335573	0.017297	0.057182	0.013471	-0.012647	0.000824	1.065153791	-16.4411
	H53-C58	5.228193	0.015084	0.05838	0.011972	-0.009348	0.002624	1.280701754	-12.1524
val455	N21-O71	5.863289	0.01143	0.042093	0.009624	-0.008725	0.000899	1.103037249	-11.3425
Phe454	N1-O71	5.516274	0.015397	0.046026	0.011016	-0.010526	0.00049	1.046551397	-13.6838

selected by virtual screening analysis along with HER2 alone. The free HER2 and HER2 in complex with COM A, COM B, and COM C were subjected to independent 30 ns

of MD simulation. MD simulation provided the details about the overall stability of unbound or inhibitor-bounded HER2 at nanosecond time scale. The RMSD, RMSF, and

Table 8. Topological Properties of the Ligand 22-HER2(COM F) Bond Critical Points (XBCPs) for all the Systems Considered

COM F	Atoms	BPL	ρ	$\nabla^2\rho$	G	V	H	-G (V)	E (kJ mol ⁻¹)
Leu452	O4-H47	4.488928	0.009311	0.036857	0.008392	-0.00757	0.000822	1.1085865	-9.841
Asn476	H31-O50	4.53379	0.012121	0.041905	0.009722	-0.008967	0.000755	1.0841976	-11.6571
	H33-O50	4.521156	0.009078	0.037354	0.008283	-0.007228	0.001055	1.1459602	-9.3964
	O23-H65	6.211915	0.001768	0.007795	0.001462	-0.000974	0.000488	1.5010267	-1.2662
	O23-H68	6.136284	0.001755	0.00766	0.001417	-0.000919	0.000498	1.5418934	-1.1947
	O23-H73	6.785641	0.001845	0.006806	0.001194	-0.000687	0.000507	1.7379913	-0.8931

Table 9. Energy Collection by the Type and Amount Tails of Receptor Binding with Complexes (A, B, C, D, E and F)

Number	Ligand 12- HER2(COM A)	Ligand 19- HER2(COM B)	Ligand 10- HER2(COM C)	Ligand 23- HER2(COM D)	Ligand 7- HER2(COM E)	Ligand 22- HER2(COM F)
E total His456 (kJ mol ⁻¹)	-77.4137	-81.8207	-40.404	0	-52	0
E total Val455 (kJ mol ⁻¹)	-97.3297	-58.5403	0	-70.0544	-23.92	0
E total PHE456 (kJ mol ⁻¹)	-13.5174	0	-60.3265	0	-13.78	0
Total Asn476 (kJ mol ⁻¹)	0	-33.9729	-9.2482	-51.7335	0	-24.4075
E total Glu479 (kJ mol ⁻¹)	-247.5707	0	0	0	0	0
Total leu452 (kJ mol ⁻¹)	0	0	0	-12.1524	0	-9.841
E total	-435.8315	-174.3339	-153.7077	-133.9403	-89.7	-34.2485

RG were occupied to evaluate the stability and mobility of the simulated system.

RMSD is a popular factor to investigate conformational

variations and estimate the stability, According to the calculated RMSD for all systems, the RMSD variation of HER2: COM A complex is higher than that of the others. At

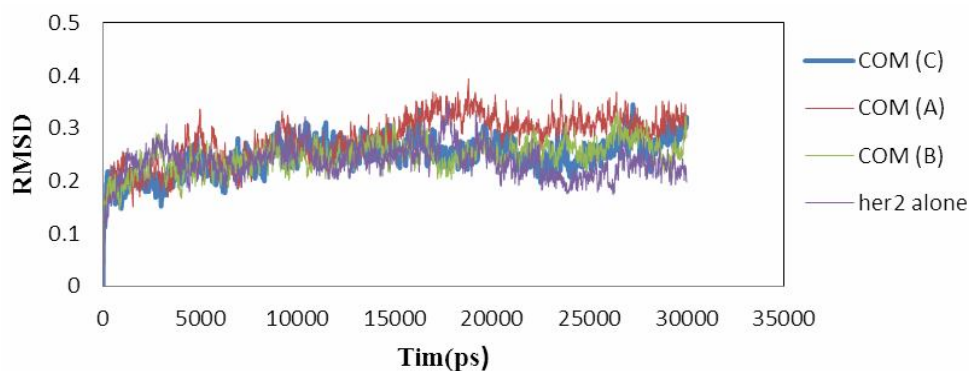


Fig. 4. The comparison of RMSD values of free HER2 (violet line), HER2-ligand10 (blue line) HER2-ligand12 (red line), and HER2-ligand19 (green line).

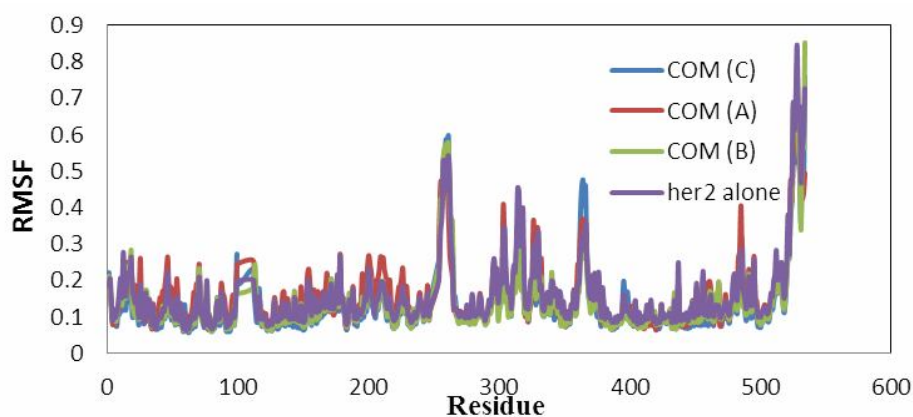


Fig. 5. The comparison of RMSF values of free HER2 (violet line), HER2-ligand10 (blue line), HER2-ligand12 (red line) and HER2-ligand19 (green line).

first, there is an increase in RMSD value to 0.31 nm around 10000 ps. Then, it decreased to 0.22 nm at 11520 ps. Subsequently, it was increased to 0.38 nm at 18780 ps (based on Fig. 4). Finally, it was reached steady state at 22000 ps with negligible changes in RMSD. On the other hand, for free HER2, the RMSD value was increased to 0.32 nm at 10000 ps. Then, a decreasing trend to 0.2 nm at 30000 ps started. The RMSD profiles of COM C and COM B at 10000-30000 ps are almost similar to each other [4,6].

According to Fig. 4, the highest and lowest mobility at 18790 and 17660 picoseconds are related to the COM A and Her2 alone, respectively. Eventually, the equilibrium state arrived at 45780 ps.

Root mean square fluctuation (RMSF). The average residue's fluctuation was calculated through root mean square fluctuation (RMSF), as presented in Fig. 5; the RMSF describes the flexibility of different residues [58]. Figure 5 shows that the N-terminus of all systems have the high flexibility, which is predictable due to being free in one side and there are four regions having significant fluctuations. A point should be taken into account is that the more flexibility of these regions can be associated with their secondary structures, which are mainly random coil, and this fact that the number of hydrogen bonds in the structure of coil is less than those in helical and β -sheet. So, the study of the residue's nature in these regions can help us to

discuss the nature of the interactions [59].

The first region consists of twenty amino acids ranging from Cys246 to Phe269. Previous studies showed that residues Leu244-Tyr267 corresponded to the dimerization loop of domain II [60]. These residues are mostly involved in turn and beta sheet structures. The nature of the involved residues is mainly polar or charged. Therefore, it can be concluded that the interactions in this region likely occur electrostatically. In the second region including thirty-three residues (Val300-Ala333), there are roughly equal amount of polar/charged residues and hydrophobic residues. Hence, in this area, there are both electrostatic and Van der Waals interactions simultaneously. In the third and fourth sections, which respectively contain 15 (Leu355 to Leu370) and 32 (ranging from Gly502-Asn534) amino acids, similarly, there are comparable amounts of polar/charged residues and hydrophobic/nonpolar residues. Therefore, it can be deduced that both electrostatic and Van der Waals interactions can occur concurrently. The most of residues in the four mentioned areas predominantly are engaged in beta sheet and turn structures.

The extracellular region of HER2 comprises four distinct domains; domain I (residues Gln2-Arg196), domain II (Thr197-Val320), domain III (Cys321-Ala489) and domain IV (Cys490-Cys566) [61]. The change in the orientations of domain I-II pair relative to the domain III-IV pair is necessary for HER2 activation. This re-orientation in the presence of an activator ligand is mediated through the rotations of residues 316-323. The largest rotation occurs about Val320 in HER2 [62]. In Fig. 5, the residues mentioned above are shown as stick presentation. In comparison with free HER2, the RMSF values of COM A and COM C were decreased. In unbound HER2, the RMSF value of Val 320 was 2.0 Å, whereas in COM A and COM C, it was reduced to 1.2 and 1.1 Å, respectively.

In the current study, the average RMSF of HER2 residues was assessed in unbound HER2, or bound with COMA and COMC MD trajectories, to study the effect of inhibitor binding on protein conformational stability. The average RMSF value of HER2 alone was 1.5 Å, while for COMA: HER2 complex and COM C: HER2 complex, the RMSFs were 1.5 and 1.3 Å, respectively. The data suggest that the binding of COM A into the HER2 has not a remarkable effect on the fluctuations of the residues. On the

contrary, upon COM C binding, the residues fluctuations were reduced probably due to the stabilizing inter-residue interactions that restrict the conformational freedom. Table S30 illustrated RMSF values for HER2 alone, COM A, COM B and COM C.

Radius of gyration (Rg). Rg is a parameter indicating the compactness of protein. To estimate the effects of different ligand bindings on protein, Rg for free HER2, and HER2 in the presence of COM A, COM B and COM C were calculated and analyzed (Fig. 6). For free HER2, there are fluctuations in the Rg curve. However, a slight decrease is seen in the curve during 30 ns MD simulation. Similarly, there is a downward trend in the Rg curves of COM C and COM A complexes. It means that in these cases HER2 protein tends to further pack. Figure 7 illustrates the superimposed presentation of free HER2, COM A: HER2 and COM C: HER2 complexes. Upon this figure, binding of COM A or COM C to HER2 made domain I and domain III close together. This rearrangement was derived through approaching the alpha helix and beta sheets located in the interface of domains I and III.

On the other hand, COM B shows the nearly constant Rg around 2.71 nm. It can be concluded that the presence of ligand19 does not allow further protein packing leading to the compactness retaining.

Binding Free Energy

Modified molecular mechanics-Poisson Boltzmann surface area (MM-PBSA) is a program written in Python to streamline end-state free energy calculations by using ensembles derived from molecular dynamics (MD) or Monte Carlo (MC) simulations. Binding free energies are calculated by subtracting the free energies of the unbound receptor and ligand from the free energy of the bound complex.

$$\Delta G_{\text{binding}} = G_{\text{complex}} - (G_{\text{protein}} + G_{\text{ligand}}) \quad (4)$$

In which G_{complex} represents the total free energy of the protein-inhibitor complex and G_{protein} and G_{ligand} are total free energies of the separated form of protein and inhibitor in solvent [63], respectively. As mentioned earlier, MM-PBSA method was used to estimate the free energy of interaction between HER2 in COM A, COM B and COM C

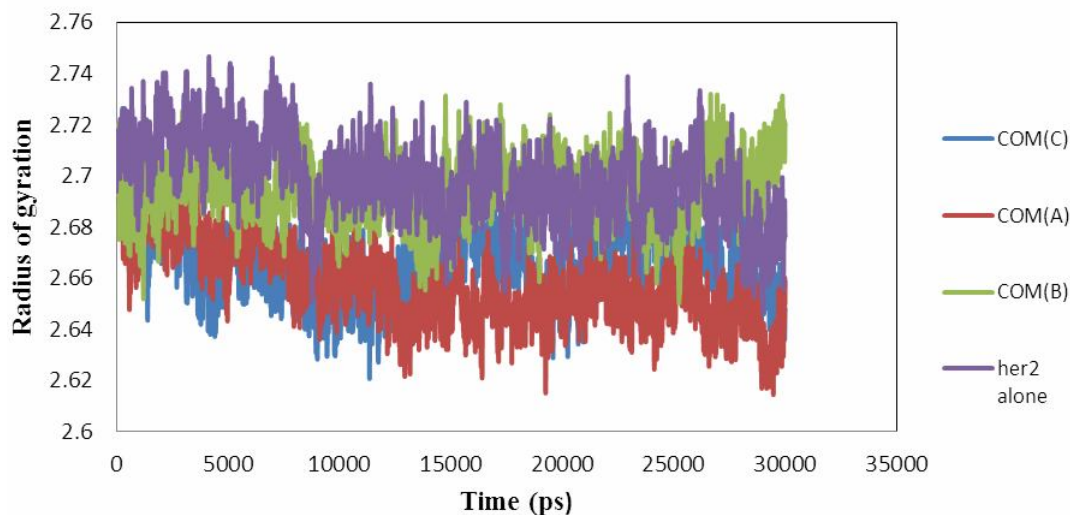


Fig. 6. The comparison of Rg values for free HER2 (violet line), Her2-ligand10 (blue line), Her2-ligand12(COM A) (red line) and Her2-ligand19 (green line) compounds.

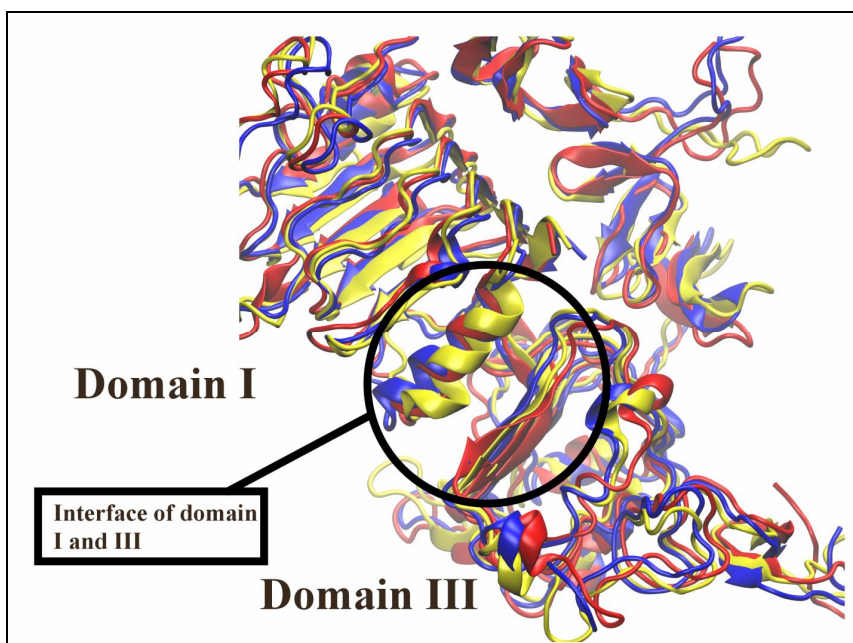


Fig. 7. The superposition of 3D structures of free HER2 (blue), COM A (red) and COM C (yellow) complexes. The superposing was done by Multiseq code in VMD.

[64]. The snapshots were extracted from the last 20 ns of MD trajectories to analyze the binding free energy. The values of binding free energy for COM A, COM B, and

COM C are given in Table 10. The obtained values show that under equal conditions, the polar and Van der Waals energies are the most effective energies playing a key role

Table 10. Molecular Energy Terms for Complexes A, B and C

Ligand 10-HER2 (COM C)	Ligand 19-HER2 (COM B)	Ligand 12-HER2 (COM A)	Energy (kcal mol ⁻¹)
-193.658 ± 15.678	0 + 0	-147.892 ± 6.635	ΔE_{vdw}
-59.778 ± 3.664	-0.138 ± 0.045	-32.776 ± 3.346	ΔE_{elect}
151.355 ± 5.841	16.784 ± 9.636	151.868 ± 10.091	ΔE_{solv}
-15.740 ± 0.847	1.737 ± 0.579	15.998 ± 10.091	ΔE_{SASA}
-117.819 ± 18.702	18.383 ± 9.011	-44.799 ± 0.982	$\Delta G_{binding}$

in binding of complex A, B and C to the binding site of HER2 (Table 10).

CONCLUSIONS

Crystal structure of the extracellular region of human HER2 complexed with Herceptin Fab (1N8Z) was retrieved from the Brookhaven protein data bank. All non-polar hydrogen atoms and water molecules were removed, and atom charges were computed using the Gasteiger-Marsili method. After finding the predicted residues and surrounding residues, the binding site in the HER2 extracellular domain was identified. The virtual screening was performed among 2000 chemicals retrieved from ZINC library to find specific inhibitors for the binding site of HER2 extracellular region. The binding site of protein was obtained using the scoring function to measure the binding affinity of the identified hits. It was found that different ligands interact with His456, Val455, Phe456, Asn476 and Glu479 residues. The strongest interaction with protein belongs to ligand 12 (COM A) with the binding energy of -435.831 kJ mol⁻¹, the ligand 22 with the binding energy value of -34.248 kJ mol⁻¹ was the weakest inhibitor.

The RMSD data showed that all systems reached the equilibrium during MD simulations. Considering the RMSF results, in the presence of COM A and COM C, flexibilities of residues 316-323 from HER2 were restricted. It was shown that the mobility of this region is necessary for the HER2 activation. Temporal Rg exhibited that upon COM A or COM C binding, the Rg of HER2 was decreased. Further

analysis showed that this decreasing belonged to approaching the domains I and III.

Based on MM-PBSA results, the bonding free energy of ligand 10 is -117.819 ± 18.702 kJ mol⁻¹ and the value obtained for the total bonding energy from quantum theory of atoms in molecules calculations is -153.708 kJ mol⁻¹.

ACKNOWLEDGEMENTS

We gratefully acknowledge the graduate Office University of Guilan for supporting of this work.

REFERENCES

- [1] Kickbusch, I., The contribution of the World Health Organization to a new public health and health promotion, *J. Am Public Health*. 2003, 93, 383-388.
- [2] Ferreira, L.; dos Santos, R.; Oliva, G., Andricopulo, A., Andricopulo, molecular docking and structure-based drug design strategies, *J. Molecules*. **2015**, 13384-13421, DOI: 10.3390/molecules200713384.
- [3] Fiszman, G. L.; Jasnis, M. A., Molecular mechanisms of trastuzumab resistance in HER2 overexpressing breast cancer, *J. Int. Cancer*. **2011**, 2011, DOI: 10.4061/2011/352182.
- [4] Motoyama, A. B.; Hynes, N. E.; Lane, H. A., The efficacy of ErbB receptor-targeted anticancer therapeutics is influenced by the availability of epidermal growth factor-related peptides, *J. Cancer Res*. **2002**, 62, 3151-3158.

- [5] Gajria, D.; Chandarlapaty, S., HER2-amplified breast cancer: mechanisms of trastuzumab resistance and novel targeted therapies, *J. Expert. Rev. Ant.* **2011**, *11*, 263-275, DOI: 10.1586/era.10.226.
- [6] Carter, P.; Presta, L. E. N.; Gorman, C. M.; Ridgway, J. B.; Henner, D., Humanization of an anti-p185HER2 antibody for human cancer therapy, *J. Proc. Natl. Acad. Sci.* **1992**, *89*, 4285-4289, DOI: 10.1073/pnas.89.10.4285.
- [7] Lane, H. A.; Motoyama, A. B.; Beuvink, I.; Hynes, N. E., Modulation of p27/Cdk2 complex formation through 4D5-mediated inhibition of HER2 receptor signaling, *J. Ann Oncol.* **2001**, *12*, S21-S22, DOI: 10.1093/annonc/12.suppl_1.S21.
- [8] Satyanarayanajois, S.; Villalba, S.; Jianchao, L.; Lin, G. M., Design, synthesis, and docking studies of peptidomimetics based on HER2-Herceptin binding site with potential antiproliferative activity against breast cancer cell lines, *J. Chem. Bio. Drug.* **2009**, *74*, 246-257, DOI: 10.1111/j.1747-0285.2009.00855.x.
- [9] Jemal, A.; Siegel, R.; Ward, E.; Hao, Y.; Xu, J.; Thun, M. J., CA: a cancer journal for clinicians, *Cancer statistics.* **2010**, *60*, 277-300, DOI: 10.3322/caac.20073.
- [10] Petit, A. M.; Rak, J.; Hung, M. C.; Rockwell, P.; Goldstein, N.; Fendly, B.; Kerbel, R. S., Neutralizing antibodies against epidermal growth factor and ErbB-2/neu receptor tyrosine kinases down-regulate vascular endothelial growth factor production by tumor cells *in vitro* and *in vivo*: angiogenic implications for signal transduction therapy of solid tumors, *J. Am. J. Pathol.* **1997**, *151*, 1523.
- [11] Wang, J.; Pursell, N. W.; Samson, M. E. S.; Atoyan, R.; Ma, A. W.; Selmi, A.; Lai, C. J., Potential advantages of CUDC-101, a multitargeted HDAC, EGFR, and HER2 inhibitor, in treating drug resistance and preventing cancer cell migration and invasion, *J. Molecular Cancer Therapeutics.* **2013**, *12*, 925-936, DOI: 10.1158/1535-7163.
- [12] Dominguez, C; Boelens, R.; Bonvin, A. M., HADDOCK: A protein-protein docking approach based on biochemical or biophysical information. *J. ACS.* **2003**, *125*, 1731-1737, DOI: 10.1021/ja026939x.
- [13] Yang, J. M.; Chen, C. C., GEMDOCK: A generic evolutionary method for molecular docking, *J. Proteins.* **2004**, *55*, 288-304, DOI: 10.1002/prot.20035.
- [14] de Azevedo, J; Walter, F.; Dias, R., Experimental approaches to evaluate the thermodynamics of protein-drug interactions, *J. Current Drug Targets.* **2008**, *9*, 1071-1076, DOI: 10.2174/138945008786949441.
- [15] Mortier, J.; Rakers, C.; Bermudez, M.; Murgueitio, M. S.; Riniker, S.; Wolber, G., The impact of molecular dynamics on drug design: applications for the characterization of ligand-macromolecule complexes, *J. Drudis.* **2015**, *20*, 686-702, DOI: 10.1016/j.drudis.2015.01.003.
- [16] Skinner, A. L.; Laurence, J. S., High-field solution NMR spectroscopy as a tool for assessing protein interactions with small molecule ligands, *J. Pharmasic.* **2008**, *97*, 4670-4695, DOI: 10.1002/jps.21378.
- [17] van Gunsteren, W. F.; Weiner, P.K.; Wilkinson, A. J., Computer simulation of biomolecular systems: theoretical and experimental applications, J. Springer Science & Business Media, 2013.
- [18] Skinner, A. L.; Laurence, J. S., Probing residue-specific interactions in the stabilization of proteins using high-resolution NMR: a study of disulfide bond compensation, *J. Pharmasic.* **2010**, *99*, 2643-2654, DOI: 10.1002/jps.22055.
- [19] Ahn, E. R.; Wang, E.; Glück, S., Is the improved efficacy of trastuzumab and lapatinib combination worth the added toxicity A discussion of current evidence, recommendations, and ethical issues regarding dual HER2-targeted therapy Breast cancer, *J. JCBR.* **2012**, *6*, 191, DOI: 10.4137/BCBCR.S9301.
- [20] Lu, S. Y.; Jiang, Y. J.; Zhou, P.; Zou, J. W.; Wu, T. X., Geometric characteristics and energy landscapes of halogen-water-hydrogen bridges at protein-ligand interfaces, *J. Chem. Phys. Lett.* **2010**, *485*, 348-353, DOI: 10.1016/j.cplett.2009.12.077.
- [21] Mirzaie, S.; Chupani, L.; Barzegari Asadabadi, E.; Shahverdi, A. R.; Jamalán, M., Novel inhibitor discovery against aromatase through virtual screening and molecular dynamic simulation: a computational

- approach in drug design, *J. Excell.* **2013**, *12*, 168-183.
- [22] Bigler, D. J.; Peterson, L. W.; Cafiero, M., Effects of implicit solvent and relaxed amino acid side chains on the MP2 and DFT calculations of ligand–protein structure and electronic interaction energies of dopaminergic ligands in the SULT1A3 enzyme active site, *J. Chem. Theory Comput.* **2015**, *1051*, 79-92, DOI: 10.1016/j.comptc.2014.10.031.
- [23] Shukla, R.; Shukla, H.; Kalita, P.; Sonkar, A.; Pandey, T.; Singh, D. B.; Kumar, A.; Tripathi, T., Identification of potential inhibitors of *Fasciola gigantica*, *J. Biomol. Struct. Dyn.* **2017**, 1-68, DOI: 10.1002/jcb.26444.
- [24] DiMasi, J. A.; Hansen, R. W.; Grabowski, H. G., The price of innovation: new estimates of drug development costs. *J. Health Econ.* **2003**, *22*, 151-185, DOI: 10.1016/S0167-6296(02)00126-1.
- [25] Arribas, J.; Baselga, J.; Pedersen, K.; Parra-Palau, J. L., p95HER2 and breast cancer, *J. Can. Res.* **2015**, *71*, 1515-1519, DOI: 10.1158/0008-5472.
- [26] Gasteiger, J.; Marsili, M., Iterative partial equalization of orbital electronegativity—a rapid access to atomic charges, *J. Tetrahedron.* **1980**, *36*, 3219-3228, DOI: 10.1016/0040-4020(80)80168-2.
- [27] Van Der Spoel, D.; Lindahl, E.; Hess, B.; Groenhof, G.; Mark, A. E.; Berendsen, H. J., GROMACS: fast, flexible, and free, *J. Comput. Chem.* **2005**, *26*, 1701-1718, DOI: 10.1002/jcc.20291.
- [28] Irwin, J. J.; Sterling, T.; Mysinger, M. M.; Bolstad, E. S.; Coleman, R. G., ZINC: a free tool to discover chemistry for biology, *J. Chem. Inf. Model.* **2012**, *52*, 1757-1768, DOI: 10.1021/ci3001277.
- [29] de Vries, S. J.; Bonvin, A. M., CPORT: a consensus interface predictor and its performance in prediction-driven docking with HADDOCK, *J. PloS One.* **2011**, *6*, e17695, DOI:10.1371/journal.pone.0017695.
- [30] Thomsen, R.; Christensen, M. H., MolDock: a new technique for high-accuracy molecular docking, *J. Med. Chem.* **2006**, *49*, 3315-3321, DOI: 10.1021/jm051197e.
- [31] De Azevedo, J.; Walter, F., MolDock applied to structure-based virtual screening, *J. Current Drug Targets.* **2010**, *11*, 327-334, DOI: 10.2174/138945010790711941.
- [32] Torktaz, I; Zahiri, H. S.; Noghabi, K. A., In silico modeling of the type 2 IDI enzymes of *Bacillus licheniformis*, *Pseudomonas stutzeri*, *Streptococcus pyogenes*, and *Staphylococcus aureus* for virtual screening of potential inhibitors of this therapeutic target, *J. Mol. Graph Model.* **2013**, *39*, 176-182, DOI: 10.1016/j.jm gm.2012.11.007.
- [33] Lagorce, D; Sperandio, O; Galons, H; Miteva, M. A.; Villoutreix, B. O., FAF-Drugs4: free ADME/tox filtering tool to assist drug discovery and chemical biology projects, *J. BMC Bioinformatics.* **2008**, *9*, 396, DOI: 10.1093/bioinformatics/btx491.
- [34] Humphrey, W.; Dalke, A.; Schulten, K., VMD: Visual molecular dynamics, *J. Mol. Graph.* **1996**, *14*, 33-38, DOI: 10.1016/0263-7855(96)00018-5.
- [35] Parrinello, M.; Rahman, A., Polymorphic transitions in single crystals: A new molecular dynamics method, *J. App. Phys.* **1981**, *52*, 7182-7190, DOI: 10.1063/1.328693.
- [36] Wang, J; Wang, W; Kollman, P. A.; Case, D. A., Automatic atom type and bond type perception in molecular mechanical calculations, *J. Mol. Graph Model.* **2006**, *25*, 247-260, DOI: 10.1016/j.jm gm.2005.12.005
- [37] Jorgensen, W. L.; Chandrasekhar, J.; Madura, J. D.; Impey, R. W.; Klein, M. L., Comparison of simple potential functions for simulating liquid water, *J. Chem. Phys.* **1983**, *79*, 926-935, DOI: 10.1063/1.445869.
- [38] Darden, T.; York, D.; Pedersen, L., Particle mesh Ewald: An N-log(N) method for Ewald sums in large systems, *J. Chem. Phys.* **1993**, *98*, 10089-10092, DOI: 10.1063/1.464397.
- [39] Essmann, U.; Perera, L.; Berkowitz, M. L.; Darden, T.; Lee, H.; Pedersen, L. G., A smooth particle mesh Ewald method, *J. Chem. Phys.* **1995**, *103*, 8577-8593, DOI: 10.1063/1.470117.
- [40] Bussi, G.; Donadio, D.; Parrinello, M., Canonical sampling through velocity rescaling, *J. Chem. Phys.* **2007**, *126*, 014101, DOI: 10.1063/1.2408420.
- [41] Ghalami-Chooabar, B.; Moghadam, H., Molecular docking based on virtual screening, molecular dynamics, and Atoms in Molecules studies to identify the potential human epidermal receptor 2 intracellular

- domain inhibitors, *J. PCR*. **2018**, *6*, 83-103, DOI: 10.22036/pcr.2017.88200.1385.
- [42] Dennington, R. D.; Keith, T. A.; Millam, J. M., GaussView 5.0. 8. Gaussian Inc., 2008.
- [43] Frisch, M. J; Trucks, G. W; Schlegel, H. B; Scuseria, G. E; Robb, M. A.; Cheeseman, J. R; Montgomery, J. A; Vreven, T; Kudin, K. N; Burant, J. C.; Millam, J. M; Iyengar, S. S; Tomasi, J., Barone, V; Mennucci, B; Cossi, M., Scalmani, G; Rega, N; Petersson, G. A; Nakatsuji, H; Hada, M., Ehara, M; Toyota, K; Fukuda, R; Hasegawa, J; Ishida, M; Nakajima, T; Honda, Y; Kitao, O; Nakai, H., Klene, M; Li, X; Knox, J. E; Hratchian, H. P; Cross, J. B; Bakken, V; Adamo, C; Jaramillo, J; Gomperts, R; Stratmann, R. E; Yazyev, O; Austin, A. J; Cammi, R; Pomelli, C; Ochterski, J. W; Ayala, P. Y; Morokuma, K; Voth, G. A; Salvador, P; Dannenberg, J. J; Zakrzewski, V. G; Dapprich, S; Daniels, A. D; Strain, M. C; Farkas, O; Malick, D. K; Rabuck, A. D; Raghavachari, K; Foresman, J. B; Ortiz, J. V; Cui, Q; Baboul, A. G; Clifford, S; Cioslowski, J; Stefanov, B. B; Liu, G; Liashenko, A; Piskorz, P; Komaromi, I., Martin, R. L., Fox, D. J; Keith, T; Laham, A; Peng, C. Y; Nanayakkara, A; Challacombe, M; Gill, P. M. W; Johnson, B; Chen, W; Wong, M. W; Gonzalez, C.; Pople, J. A., Gaussian 03, Revision C.02., 2003.
- [44] Frisch, M. J.; Trucks, G. W.; Schlegel, H. B.; Scuseria, G. E.; Robb, M. A.; Cheeseman, J. R.; Montgomery Jr, J. A.; Vreven, T.; Kudin, K. N.; Burant, J. C.; Millam, J. M., Gaussian 03, revision B. 05; Gaussian, Inc., Pittsburgh, PA, DOI: 2003.
- [45] Becke, A. D., Density-functional thermochemistry. III. The role of exact exchange, *J. Chem. Phys.* **1993**, *98*, 5648-5652, DOI: 10.1063/1.464913.
- [46] Lee, C.; Yang, W.; Parr, R. G., Development of the Colle-Salvetti correlation-energy formula into a functional of the electron density, *J. Phys. Rev. B*. **1998**, *37*, 785, DOI: 10.1103/PhysRevB.37.785.
- [47] Peng, C.; Ayala, P. Y.; Schlegel, H. B.; Frisch, M. J., Using redundant internal coordinates to optimize equilibrium geometries and transition states, *J. Comput. Chem.* **1996**, *17*, 49-56 [48] Espinosa, E.; Molins, E., Retrieving interaction potentials from the topology of the electron density distribution: The case of hydrogen bonds, *J. Chem. Phys.* **2000**, *113*, 5686-5694, DOI: 0.1063/1.1290612.
- [48] Bader, R. F. W., Atoms in molecules: a quantum theory. International series of monographs on chemistry 22, Oxford University Press, Oxford, 1990.
- [49] T. Keith, AIMAll (Version 13.02. 26), TK Gristmill Software, DOI 2012.
- [50] Espinosa, E.; Souhassou, M.; Lachekar, H.; Lecomte, C., Topological analysis of the electron density in hydrogen bonds, *J. Acta Crys. Sect. B*. **1999**, *55*, 563-572, DOI: 10.1107/S0108768199002128.
- [51] Gatti, C.; Saunders, V.; Roetti, C., Crystal field effects on the topological properties of the electron density in molecular crystals: the case of urea, *J. Chem. Phys.* **1994**, *101*, 10686-10696, DOI: org/10.1063/1.467882 C. Gatti.
- [52] Cremer, D.; Kraka, E, Chemical bonds without bonding electron density-does the difference electron-density analysis suffice for a description of the chemical bond?, *J. Angew. Chem. Int. Ed. Engl.* **1984**, *23*, 627-628, DOI: org/10.1002/anie.198406271.
- [53] enkins, S.; Morrison, I., The chemical character of the intermolecular bonds of seven phases of ice as revealed by ab initio calculation of electron densities, *J. Chem. Phys. Lett.* **2000**, *317*, 97-102, DOI: 10.1016/S0009-2614(99)01306-8.
- [54] Grabowski, S. J., High-level *ab initio* calculations of dihydrogen-bonded complexes, *J. Phys. Chem. A*. **2000**, *104*, 5551-5557, DOI: org/10.1021/jp993984r.
- [55] Vener, M. V.; Manaev, A. V.; Egorova, A. N.; Tsirelson, V. G., QTAIM study of strong H-bonds with the OH A fragment (A = O, N) in three-dimensional periodical crystals, *J. Phys. Chem. A*. **2007**, *111*, 1155-1162, DOI: 10.1021/jp067057d.
- [56] Arnold, W. D.; Oldfield, E., The chemical nature of hydrogen bonding in proteins via NMR: J-couplings, chemical shifts, and AIM theory, *J. Am. Chem. Soc.* **2000**, *122*, 12835-12841, DOI: 10.1021/ja0025705.
- [57] Kumar, K.; Anbarasu, A.; Ramaiah, S., Molecular docking and molecular dynamics studies on β -lactamases and penicillin binding proteins, *J. Mol. Bio Syst.* **2014**, *10*, 891-900, DOI: 10.1039/C3MB70537D.
- [58] Chegini, H.; Beyramabadi, S. A.; Morsali, A.; Saberi,

- M.; Lotfi, M., QTAIM study of substituent effects on the intramolecular hydrogen bond in 3, 3'-dihydroxy-4,4'-[5-methyl-1,3-phenylenebis(nitrilomethylidyne)]-bis-phenol, *J. Mol. Struct.* **2015**, *1083*, 1-9, DOI: 10.1016/j.molstruc.2014.11.031.
- [59] Niazi, S.; Purohit, M.; Sonawani, A.; Niazi, J. H., Revealing the molecular interactions of aptamers that specifically bind to the extracellular domain of HER2 cancer biomarker protein: An in silico assessment, *J. Mol. Graph. Model.* **2018**, *83*, 112-121.
- [60] D'Huyvetter, M.; De Vos, J.; Xavier, C.; Pruszyński, M.; Sterckx, Y. G.; Massa, S.; Raes, G.; Cavellers, V.; Zalutsky, M. R.; Lahoutte, T.; Devoogdt, N., 131I-labeled anti-HER2 camelid sdAb as a theranostic tool in cancer treatment, *J. Clin. Cancer Res.* **2017**, *23*, 6616-28, DOI: 10.1158/1078-0432.CCR-17-0310.
- [61] Cho, H. S.; Mason, K.; Ramyar, K. X.; Stanley, A. M.; Gabelli, S. B.; Denney Jr, D. W.; Leahy, D. J., Structure of the extracellular region of HER2 alone and in complex with the Herceptin Fab, *J. Nature.* **2003**, *421*, 6924, p.756, DOI: 10.1038/nature01392.
- [62] MM, S. M., Molecular dynamics and high throughput binding free energy calculation of anti-actin anticancer drugs-new insights for better design, *J. Comput. Biol. Chem.* **2016**, *64*, 47-55, DOI: 10.1016/j.compbiochem.2016.05.008.
- [63] Kumari, R.; Kumar, R.; Lynn, A., Gmmpbsa A GROMACS tool for hgh-throughput MM-PBSA calculations, *J. Chem. Inf. Model.* **2014**, *54*, 1951-1962, DOI: 10.1021/ci500020m.